RESEARCH ARTICLE | JANUARY 05 2023

Strain-mediated electric-field control of the electronic transport properties of 5d iridate thin films of SrIrO$_3$ ⊘

Shuang-Shuang Li ; Ying Zhang; Jing-Shi Ying; Zao-Cai Wang ; Jian-Min Yan ; Guan-Yin Gao ; Mao Ye ✉ ; Ren-Kui Zheng ✉

Check for updates

View Online

Export Citation

Strain-mediated electric-field control of the electronic transport properties of 5d iridate thin films of SrIrO₃

View Online   Export Citation   CrossMark

Shuang-Shuang Li,[1] (ID) Ying Zhang,[1] Jing-Shi Ying,[1] Zao-Cai Wang,[1] (ID) Jian-Min Yan,[2] (ID) Guan-Yin Gao,[3] (ID)
Mao Ye,[4,a] and Ren-Kui Zheng[4,a] (ID)

AFFILIATIONS

[1]School of Physics and Materials Science and Jiangxi Engineering Laboratory for Advanced Functional Thin Films, Nanchang University, Nanchang 330031, China
[2]Department of Applied Physics, The Kong Polytechnic University, Hong Kong, China
[3]Hefei National Laboratory for Physical Sciences at the Microscale, University of Science and Technology of China, Hefei 230026, China
[4]School of Physics and Materials Science, Guangzhou University, Guangzhou 510006, China

[a]Authors to whom correspondence should be addressed: zrk@ustc.edu and yem001@gzhu.edu.cn

ABSTRACT

SrIrO₃ (SIO) thin films were epitaxially grown on (001)-oriented 0.7Pb(Mg$_{1/3}$Nb$_{2/3}$)O₃-0.3PbTiO₃ (PMN-PT) single-crystal substrates. Upon applying electric fields to the piezoelectric PMN-PT along the thickness direction, the electronic transport properties of SIO films can be *in situ* tuned and modulated by non-180° ferroelectric domain rotation-induced strain, piezoelectric strain, and rhombohedral-to-tetragonal structural phase transition-induced strain in the PMN-PT layer, respectively. Moreover, the weak negative magnetoresistance (MR) of the 60-nm SIO films could be modified by applying an electric field to the PMN-PT layer. At $T = 2$ K, upon the application of $E = 4$ kV/cm to the PMN-PT, MR at $H = 9$ T is reduced by 14.2% as compared to that under zero electric field, indicating in-plane compressive strain-induced suppression of the influence of quantum corrections to the conductivity in the SIO film. These results demonstrate that the electric-field controllable lattice strain is a simple approach to get insight into the strain-property relationships of 5d iridate thin films.

I. INTRODUCTION

Recently, 5d transition-metal compounds with strong spin–orbit coupling have received an increasing amount of attention because of the experimental findings and theoretical prediction of a range of fascinating phenomena such as the quantum metal-insulator transition,[1] Fermi-arc surface states,[2] anisotropic magnetoresistance (MR),[3] weak antilocalization,[4] chiral magneto-transport,[5] quantum spin Hall effect,[6] and type-II Weyl fermions.[7] One of the interesting 5d transition-metal compounds is the Ruddlesden–Popper phase of strontium iridates with the general formula Sr$_{n+1}$Ir$_n$O$_{3n+1}$ ($n = 1$, 2, and ∞).[8–15] The Sr₂IrO₄ ($n = 1$) compound was demonstrated to be a $J_{eff} = 1/2$ antiferromagnetic Mott insulator with weak ferromagnetism below $T_N = 240$ K.[11] The Sr₃Ir₂O₇ ($n = 2$), however, is barely an insulator and displays a

ferromagnetic state with a Curie temperature $T_C = 285$ K.[12] With the increasing number of IrO₂ planes to ∞, perovskite SrIrO₃ (SIO) ($n = ∞$) possesses a larger bandwidth of 1.01 eV and a three-dimensional spin–orbital correlated metallic state with a large effective mass.[16] Yoo *et al.*[17] observed a proximity-induced magnetism in a SrIrO₃ film using a La$_{0.7}$Sr$_{0.3}$MnO₃ manganite film as a neighboring layer, which yields an anomalous Hall conductivity and Hall angle as high as those observed in bulk transition-metal ferromagnets. Very recently, Jaiswal *et al.*[18] also observed a proximity-induced ferromagnetic state in a SrIrO₃ film via interfacial charge transfer using a LaCoO₃ ferromagnetic insulator film as a neighboring layer, which yields an anomalous Hall effect, fourfold symmetric anisotropic magnetoresistance, and strong magnetocrystalline. Hao *et al.*[19] found that the interlayer exchange coupling

strength and sign can be artificially modulated by varying the layer number of the SrTiO$_3$ block in [(SrIrO$_3$)$_1$/SrTiO$_3$]m (m = 1, 2, and 3) superlattices. These results demonstrate that SIO films and superlattices are interesting material systems to study the coupling effects among spin, charge, and lattice degrees of freedom.

As of now, a variety of experimental and theoretical techniques including electronic transport,[10] angle-resolved photoemission spectroscopy,[14] hydrostatic pressure effect,[20] and first-principles calculations[21] demonstrated that subtle structural changes (e.g., IrO$_6$ rotation[22]) could lead to significant changes in the band structure and electronic properties of SIO films. It is, thus, expected that the substrate-induced lattice strain is a useful tool to tune the electronic properties of SIO films. Until now, the lattice strain effects of SIO films grown on several single-crystal substrates [e.g., DyScO$_3$,[13,20] SrTiO$_3$,[14] GdScO$_3$,[23] LaAlO$_3$,[24] NdGaO$_3$,[24] and (La,Sr)(Al,Ti)O$_3$,[24]] with in-plane compressive and tensile strains have been studied by several groups. Gruenewald et al.[25] and Biswas et al.[13] found that the substrate-induced in-plane compressive stain gives rise to a metal-insulator transition in SIO films and the insulating state is always observed in thinner films with larger compressive strain. In contrast, the effects of lattice strain on the electronic properties of SIO films in the in-plane tensile strain region are rarely reported and still not well understood.

Besides the epitaxial strain, the electronic properties of SIO films are also sensitive to thin-film growth parameters. For example, either a metallic or insulating ground state has been obtained by controlling the growth temperatures.[23] Moreover, the electronic properties of SIO films are sensitive to slight chemical composition deviation from the ideal film stoichiometry and lithographic processing and are subject to degradation over time in ambient conditions,[26] which highlights that particular care is required during film growth, characterization, and processing. All these complications make it difficult to obtain intrinsic lattice strain effects since unfavorable factors (e.g., inhomogeneous distribution of Ir element,[23] compositional non-stoichiometry,[26] disorder,[27] defects,[28] etc.) that considerably affect the electronic properties of SIO films may vary from a sample to a sample. To obtain a more in-depth understanding of the lattice strain effects in SIO films, it is necessary to in situ solely tune and modulate the lattice strain of the same SIO thin-film sample in a reversible manner so that certain effects due to the above-mentioned unfavorable factors could be kept fixed.

In this context, we note that perovskite $(1 − x)$Pb(Mg$_{1/3}$Nb$_{2/3}$)O$_3$-xPbTiO$_3$ single crystals ($a \approx b \approx c \approx 4.02$ Å) possess superior ferroelectric ($2P_r \sim$ 60–80 pC/N[29]) and piezoelectric ($d_{33} \sim$ 1500–4500 pC/N[30]) properties that could be exploited for this purpose. Therefore, in this paper, we grew SIO epitaxial thin films with thicknesses ranging from 7.5 to 90 nm on 0.7Pb(Mg$_{1/3}$Nb$_{2/3}$)O$_3$–0.3PbTiO$_3$ (PMN-PT) single-crystal substrates and in situ tune and modulate the lattice strain of SIO films through electric-field-controllable ferroelectric domain rotation, converse piezoelectric effect, and rhombohedral-to-tetragonal structural phase transition of PMN-PT. Using these approaches, we are able to in situ reversibly modify the electronic properties of SIO films, providing another way to probe into the intrinsic charge-lattice coupling effects of perovskite 5d iridate compounds.

II. EXPERIMENT

The SIO ceramic target was synthesized using the solid-state reaction method. The starting materials of SrCO$_3$ (99.7%) and IrO$_2$ (99.9%) were weighed in stoichiometric amounts and ball milled in ethanol for 24h. The mixtures were dried and calcinated at 1000 °C for 24h. The calcinated mixtures were ball milled again in ethanol for 24h as well as dried, pelletized, and sintered at 1100 °C for 24h. The powder x-ray diffraction (XRD) pattern of the SIO target shows that all diffraction peaks can be indexed based on the monoclinic SrIrO$_3$ phase (PDF#72-0855) (Fig. S1 in the supplementary material).

SIO films were grown on one-side polished PMN-PT (001) substrates by pulsed laser deposition using a KrF excimer laser (λ = 248 nm). Film deposition was carried out at a substrate temperature of 750 °C and an oxygen pressure of 25 Pa. The laser energy density and repetition rate are 1.5 J/cm^2 and 3 Hz, respectively. After deposition, SIO films were in situ annealed in 1 atm oxygen atmosphere for 30 min before cooling down to room temperature at a rate of 5 °C/min.

Crystallographic properties of the SIO films were measured by x-ray diffraction (XRD) θ–2θ and φ scans using a high-resolution PANalytical X'Pert PRO x-ray diffractometer with Cu Kα1 radiation (λ = 1.5406 Å). High-angle annular dark-field scanning transmission electron microscopy (HAADF-STEM) images were measured using a FEI titan themis 200 transmission electron microscope. The specimen for HAADF-STEM measurements was prepared using a FEI Helios 450S dual beam focused ion beam (FIB).

The resistance of SIO films was measured through the four-probe technique using a physical property measurement system (PPMS) (Quantum Design). Silver (Ag) films with a thickness of 100 nm were deposited onto the SIO films to form four ohmic contact electrodes. Using the conducting SIO film and the silver film as top and bottom electrodes, respectively, initial poling and the following polarization direction switching as well as the converse piezoelectric effect were achieved by applying electric voltages to the PMN-PT substrates along the thickness direction, as schematically illustrated in the insets of Figs. 2(a) and 2(b).

III. RESULTS AND DISCUSSION

Figure 1 summarizes the structural properties of a 60-nm SIO film grown on a PMN-PT (001) substrate. From the x-ray diffraction (XRD) θ–2θ scan pattern, one can find that the (00l) (l = 1 and 2) diffraction peaks from the PMN-PT substrate and (ll0) (l = 1 and 2) diffraction peaks from the SIO film appear similar to the situation of SIO films grown on SrTiO$_3$ substrates.[31,32] No additional diffraction peaks from the SIO film could be detected within the resolution limit of the diffractometer. The XRD φ scan patterns taken from the SIO (020) and PMN-PT (101) diffraction peaks [left insets of Fig. 1(a)] suggest that the SIO film has the same fourfold symmetry as that of the PMN-PT substrate, indicating that the SIO film has been epitaxially grown on the PMN-PT substrate and the in-plane epitaxial relationship can be written as [110]SIO//[001]PMN-PT and [001]SIO//[010]PMN-PT.[31,32] The XRD ω-scan measurement taken on the SIO (220) diffraction peak yields a rocking curve with a full width at half maximum (FWHM) of 1.2°, indicating relatively good crystallinity of the film. The XRD reciprocal space mapping (RSM) pattern in the vicinity of the SIO (420) and PMN-PT (103) diffraction peaks, as
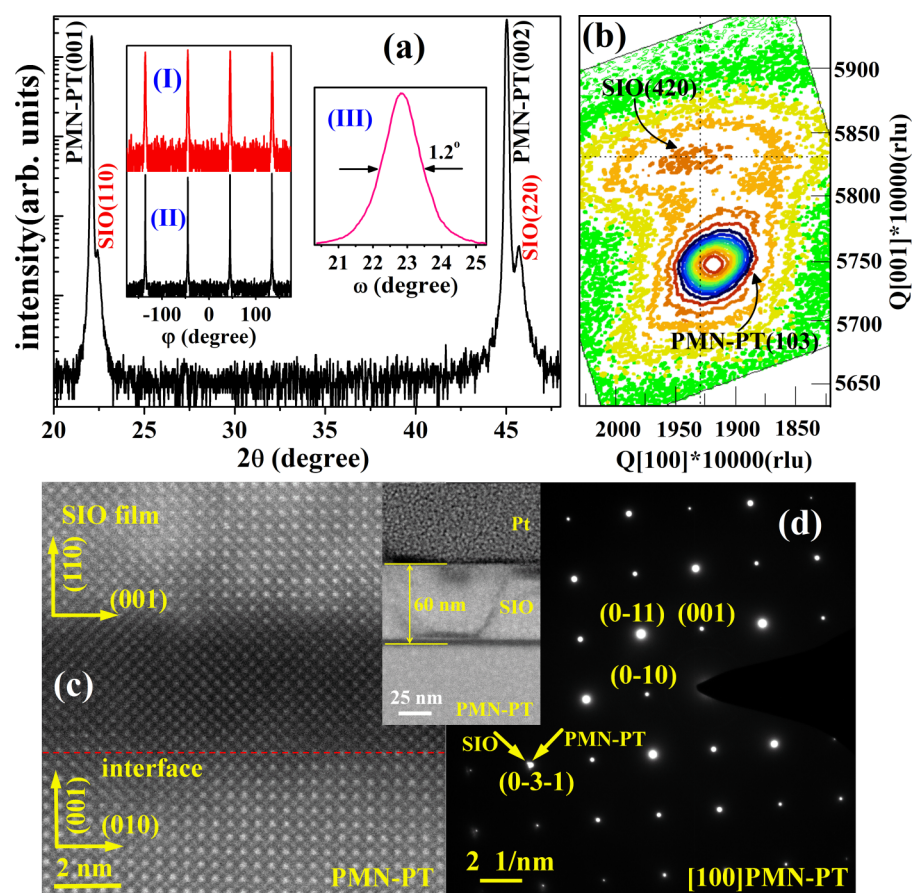
06 January 2025 06:51:21

FIG. 1. (a) XRD θ–2θ scan pattern of the 60-nm SIO/PMN-PT structure. Insets (I) and (II): XRD φ-scan patterns of the SIO film and PMN-PT substrate, respectively. Inset (III): XRD rocking curve of the SIO film. (b) RSM pattern of the SIO film and the PMN-PT substrate. (c) A cross-sectional HAADF-STEM image of the SIO/PMN-PT structure. (d) A SAED pattern taken near the interface of the SIO/PMN-PT structure. Inset: a cross-sectional TEM image of the SIO/PMN-PT structure.

shown in Fig. 1(b), gives evidence that the SIO film is coherently grown on the PMN-PT substrate. Based on (420) reflection, the in-plane and out-of-plane lattice constants of the SIO film are calculated to be ~3.996 and 3.964 Å, respectively. The in-plane lattice constant is larger than that of the SIO bulk (pseudocubic lattice parameter $a_{pc} \sim 3.959$ Å[33]) and is close to that of the PMN-PT ($a_{pc} \sim 4.02$ Å) substrate, which suggests that the SIO film is subjected to a slight in-plane tensile strain of ~0.93%. Correspondingly, the out-of-plane lattice constant should be smaller than that of the SIO bulk according to Poisson's effect. Actually, the out-of-plane lattice constant is slightly (~0.13%) larger than that of the SIO bulk, which could be caused by oxygen deficiency in the film. Note that RSM measurements reveal that SIO films with other thicknesses (7.5, 15, 30, and 90 nm) were also coherently grown on PMN-PT substrates (Figs. S2–S5 in the supplementary material). We further investigated the atomic and interface structures of the 60-nm SIO/PMN-PT structure via HAADF STEM. Figure 1(c) shows a STEM image taken near the interface region. The image displays coherent growth of the SIO film on the PMN-PT substrate and shows clear lattice fringes. There is a darker layer with a thickness of ~4 nm between the upper SIO layer and the PMN-PT substrate, which is probably caused by the rough surface due to ferroelectric domains of PMN-PT. The corresponding selected-area electron diffraction (SAED) pattern is shown

in Fig. 1(d), where sharp diffraction spots from PMN-PT can be clearly identified. The (0-3-1) diffraction spot of the SIO film can be resolved, as indicated in the SAED pattern. These structural characterizations suggest that (110)-oriented SIO thin films have been epitaxially grown on PMN-PT (001) substrates.

Figure 2(a) shows the relative resistance change ($\Delta R/R$) of the 60-nm SIO film as a function of the electric field (E) applied to the PMN-PT substrate, as measured using the schematic illustration shown in the inset of Fig. 2(a). Here, we define the electric-field induced $\Delta R/R = [R(E) - R(0)]/R(0) \times 100\%$, where $R(E)$ and $R(0)$ are resistances of the SIO film in the presence of an electric field and zero electric field, respectively. $\Delta R/R$ decreases gently with increasing electric field from zero electric field to ~3 kV/cm and shows a rapid decrease near the coercive field of the PMN-PT (~3−4 kV/cm). For $E \geq 5$ kV/cm, $\Delta R/R$ decreases approximately linearly with the applied electric field. The overall resistance behaviors are similar to our previously reported results on perovskite manganite film/PMN-PT structures[34–36] where a rapid decrease in the resistance near the near coercive field is caused by the electric-field-induced in-plane compressive strain in the PMN-PT, which is achieved through the rotation of ferroelectric domains toward the electric-field direction. To demonstrate the correlation between the lattice strain and $\Delta R/R$, the electric-field-induced
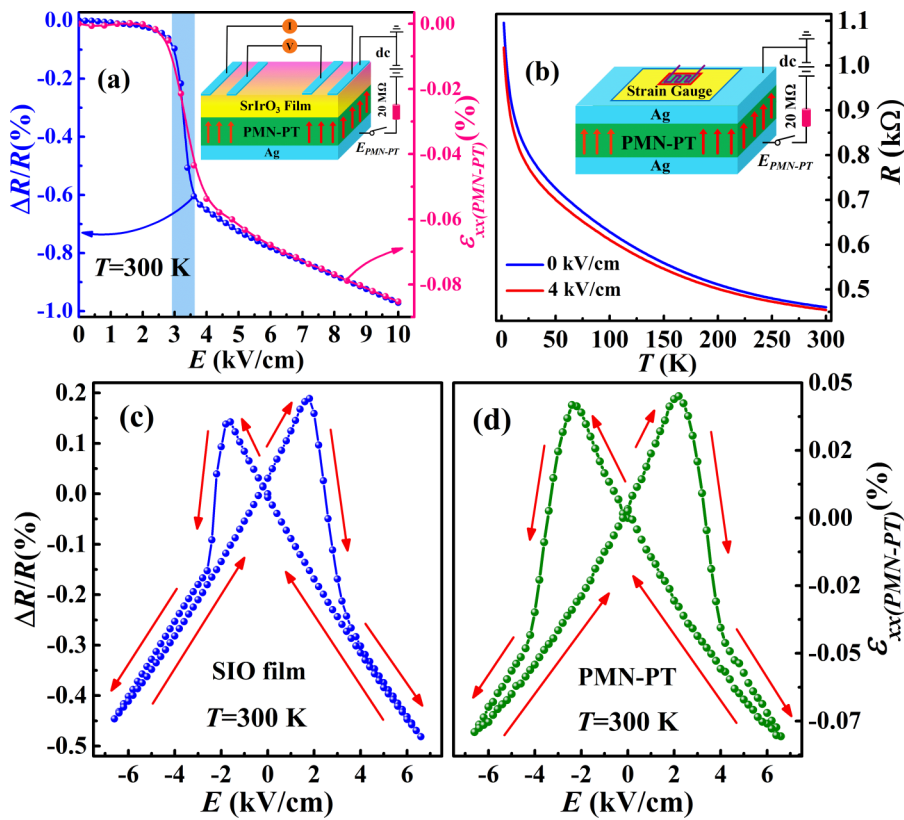
FIG. 2. (a) The relative resistance changes of the 60-nm SIO thin film ($\Delta R/R$) and the in-plane strain of the PMN-PT substrate ($\varepsilon_{xx(PMN-PT)}$) as a function of positive electric fields applied to the 60-nm SIO/PMN-PT structure, where the PMN-PT is initially in the unpolarized state. Inset: a schematic of the experimental setup for the measurements of the resistance of SIO films by applying electric fields to PMN-PT substrates. (b) Temperature dependence of the resistance of the 60-nm SrIrO$_3$ film under zero electric field and an electric field of 4 kV/cm. Inset: a schematic of the experimental setup for the measurements of the electric-field-induced $\varepsilon_{xx(PMN-PT)}$. (c) $\Delta R/R$ of the 60-nm SIO film as a function of the electric fields applied to the PMN-PT substrate. (d) $\varepsilon_{xx(PMN-PT)}$ as a function of electric fields applied to the PMN-PT substrate.

in-plane strain of the PMN-PT [ε_{PMN-PT}] was measured using a strain gauge that is attached to the top surface of a PMN-PT substrate, as schematically shown in the inset of Fig. 2(b). As also shown in Fig. 2(a), the variation trend of $\varepsilon_{xx(PMN-PT)}$ with the electric field is very similar to that of $\Delta R/R$, directly indicating that the variation of the resistance ($\Delta R/R$) is associated with $\varepsilon_{xx(PMN-PT)}$, which would be partially transferred to the neighboring SIO film via the epitaxial strain and thus modify the in-phase and antiphase tilt of the IrO$_6$ octahedra[20] and shorten the Ir–O bond distance with increasing in-plane compressive strain from the PMN-PT substrate. Figure 2(b) shows the temperature dependence of the resistance of the 60-nm SIO film under a zero electric field and an electric field of 4 kV/cm. Note that the electric field was applied to the PMN-PT substrate during the measurements of the resistance as a function of temperature. The resistance increases with decreasing temperature and shows semiconducting behaviors ($dR/dT < 0$), which is similar to that of SrIrO$_3$ and CaIrO$_3$ films under tensile strain[20,33,37] and is probably caused by the static in-plane tensile strain, oxygen deficiency, disorder, and ferroelectric-domain-caused deterioration in the crystalline quality over the whole SIO thin-film sample. Upon the application of $E = 4$ kV/cm to the PMN-PT substrate, the resistance of the SIO film decreases appreciably in the whole temperature region (2–300 K). These electric-field-induced strain effects are similar to the hydrostatic-pressure-induced strain effects in the SIO/DyScO$_3$ structure where the resistivity of the SIO film is reduced by ~7.2% through applying a 2.65 GPa pressure.[20]

To further understand the lattice strain effect in the SIO/PMN-PT structure, we measured $\Delta R/R$ of the 60-nm SIO film at various temperatures by applying bipolar electric fields to the PMN-PT substrate using the schematic of the experimental setup shown in Fig. 2(a). Note that the R vs E curve for the 60-nm SIO film and $\Delta R/R$ vs E curves for SIO films with other thicknesses (7.5, 15, 30, and 90 nm) are shown in Figs. S6–S10 in the supplementary material, respectively. For $T = 300$ K, the $\Delta R/R$ vs E curve displays a butterfly-like shape [Fig. 2(c)], which is also similar to those observed in perovskite manganites film/PMN-PT structures,[34–36] and is due to the piezoelectric strain [$\varepsilon_{xx(PMN-PT)}$] in the PMN-PT.[34] We measured $\varepsilon_{xx(PMN-PT)}$ as a function of bipolar electric fields applied to the PMN-PT substrate using the schematic of the experimental setup shown in Fig. 2(b). As shown in Fig. 2(d), $\varepsilon_{xx(PMN-PT)}$ vs E curves also show a butterfly-like shape. Therefore, it is concluded that the piezoelectric strain is the origin of the butterfly-like resistance behaviors of the SIO film.

We further studied the effects of piezoelectric strain on the resistance of the 60-nm SIO film by applying positive electric fields to the SIO/PMN-PT structure where the PMN-PT is already positively polarized and the polarization direction points to the SIO film. As shown in the inset of Fig. 3(a), for 120 K $\leq T \leq 320$ K, $\Delta R/R$ decreases linearly with increasing electric fields. According to $\varepsilon_{xx(PMN-PT)} = -d_{31}E$, where d_{31} is the transverse piezoelectric coefficient, the applied electric fields induce linear compressive $\varepsilon_{xx(PMN-PT)}$, which would be simultaneously transferred to the SIO
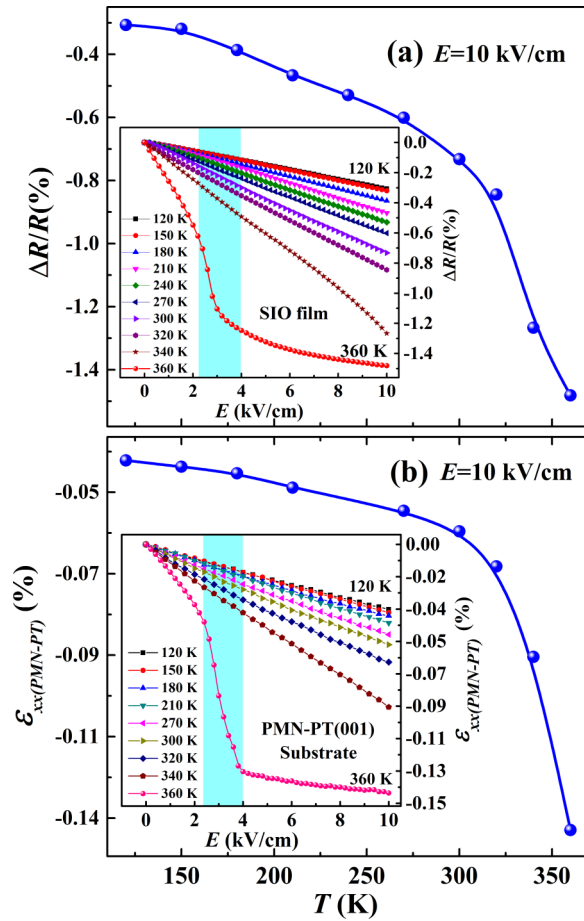
FIG. 3. (a) Temperature dependence of $\Delta R/R$ at 10 kV/cm for the 60-nm SrIrO$_3$ film. Here, $\Delta R/R$ is derived from the data shown in the inset in (a). Inset: the resistance of the 60-nm SrIrO$_3$ film as a function of the positive electric fields applied to the positively polarized PMN-PT substrate at various fixed temperatures. (b) Temperature dependence of the in-plane strain of PMN-PT ($\varepsilon_{xx(PMN-PT)}$) at 10 kV/cm. Here, $\varepsilon_{xx(PMN-PT)}$ is derived from the data shown in the inset in (b). Inset: $\varepsilon_{xx(PMN-PT)}$ as a function of positive electric fields applied to the positively polarized PMN-PT substrate at various fixed temperatures.
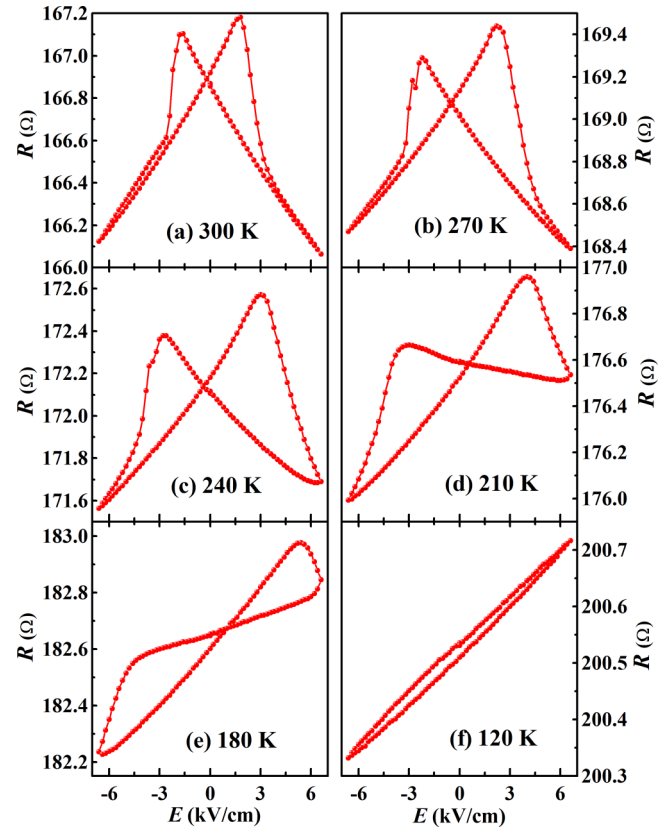

FIG. 4. The resistance of the 60-nm SIO film as a function of the bipolar electric fields applied to the PMN-PT substrate at fixed temperatures of (a) 300, (b) 270, (c) 240, (d) 210, (e) 180, and (f) 120 K.

film and thus modify the lattice strain and Ir–O–Ir bond angle and/or Ir–O distance. For $T = 340$ K, $\Delta R/R$ decreases linearly in the low field region and slightly deviates from linearity in the high field region ($E > 6$ kV/cm). For $T = 360$ K, $\Delta R/R$ decreases rapidly in the electric field region of 2.3 kV/cm $\leq E \leq 3.5$ kV/cm, where the electric-field-induced rhombohedral-to-tetragonal structural phase transition occurs.[38] We extracted the $\Delta R/R$ data at $E = 10$ kV/cm for each temperature and plotted them as a function of temperature in Fig. 3(a). $\Delta R/R$ increases with increasing temperature and reaches a maximum value of -1.6% at $T = 360$ K. To better understand the relationship between $\Delta R/R$ and the piezoelectric strain, $\varepsilon_{xx(PMN-PT)}$ was measured at the same temperatures as $\Delta R/R$ was measured. As shown in the inset of Fig. 3(b), $\varepsilon_{xx(PMN-PT)}$ shows a similar variation trend as that of $\Delta R/R$. Particularly,

$\varepsilon_{xx(PMN-PT)}$ shows a rapid decrease in the same electric-field region as that of $\Delta R/R$ at $T = 360$ K. $\varepsilon_{xx(PMN-PT)}$ at $E = 10$ kV/cm is also extracted to plot against temperature in Fig. 3(b). $\varepsilon_{xx(PMN-PT)}$ also increases with increasing temperature and shows the maximum value at $T = 360$ K, showing a similar variation trend as $\Delta R/R$. All these results demonstrate that the piezoelectric strain controls the changes of the resistance of the SIO film by applying electric fields to PMN-PT.

From Figs. 4(a)–4(f), one can find that with decreasing temperature, the R vs E curves change from a symmetrical butterfly-like shape to a slender shape. To clarify the origin of the asymmetric butterfly-like R vs E curves at low temperatures, the electric-field-induced in-plane strain of a PMN-PT substrate [$\varepsilon_{xx(PMN-PT)}$] was measured as a function of bipolar E at the same temperatures as $\Delta R/R$ was measured. The $\varepsilon_{xx(PMN-PT)}$ vs E curves also change from a butterfly-like shape to a slender shape with decreasing temperature [Figs. 5(a)–5(f)], and their variation trend is similar to that of R vs E curves, demonstrating that the piezoelectric strain-driven nature of the resistance changes at low temperatures. For a lower temperature (120 K), the R vs E curve [Fig. 4(f)] is almost linear, which is similar to the nearly linear $\varepsilon_{xx(PMN-PT)}$ vs

E curve, as shown in Fig. 5(f). Such a linear $\varepsilon_{xx(PMN-PT)}$ vs E curve is due to the increase in the coercive field of PMN-PT at a lower temperature,[39] making the electric field of 6 kV/cm unable to reverse the polarization direction of PMN-PT. It is known that the static lattice strain achieved through the growth of SIO films on different types of substrates can modify the in-plane Ir–O–Ir bond and/or Ir–O distance and, thus, tune the electronic transport properties. Our approach of using the ferroelectric domain rotation and piezoelectric strain enables *in situ* tuning of the electronic transport properties of 5d iridates, which provides a supplementary approach to understand the interactions between the lattice and the charge degrees of freedom of 5d iridates.

Next, we studied the effects of structural phase transition of PMN-PT on the electronic properties of the 60-nm SIO film. We measured the resistance of the SIO film in the temperature region of 300–390 K. From Fig. 6(a), one can observe that the resistance of the SIO film decreases with increasing temperature and shows an appreciable drop near 377 K under zero electric field, where the PMN-PT substrate undergoes a spontaneous rhombohedral-to-tetragonal structural phase transition, as revealed by the dielectric peak at $T = 378$ K (Fig. S11 in the supplementary material). According to the temperature dependence of the dielectric constant of the present PMN-PT and other PMN-PT single crystals with

similar composition,[40] the structural phase transition temperature decreases with an increasing electric field applied to PMN-PT, which causes a decrease in the temperatures where the resistance drops significantly, as shown in Fig. 6(b). Thus, it is concluded that the significant drop in the resistance is associated to the structural phase transition of the PMN-PT substrate. We note that a similar effect of structural phase transition on the electronic transport properties has been observed in La$_{0.5}$Ca$_{0.5}$MnO$_3$/Pb(In$_{1/2}$Nb$_{1/2}$)O$_3$-Pb(Mg$_{1/3}$Nb$_{2/3}$)O$_3$-PbTiO$_3$[39] and La$_{0.7}$Sr$_{0.3}$MnO$_3$/PMN-PT structures.[41] For the strong spin–orbital coupled 5d iridates, the Ir–O–Ir bond angle can be tuned by static lattice strain,[14] which, as a result, affects the electronic transport properties of iridates. Our results demonstrate that the electronic properties of SIO films can be *in situ* tuned by the electric-field-controllable structural phase transition of the PMN-PT substrate.

Finally, we investigate the effects of the electric-field-induced piezoelectric strain on the magnetotransport properties of the 60-nm SIO film and show the results in Fig. 7. Under zero electric field, the SIO film shows a negative MR at $T = 2$ K. Here, MR is
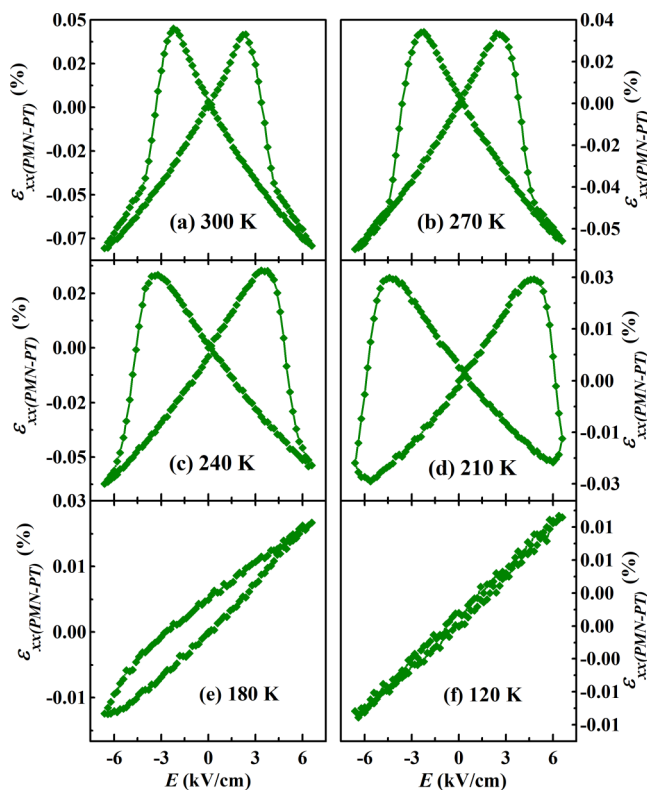

FIG. 5. The in-plane strain of the PMN-PT substrate as a function of bipolar electric fields applied to the PMN-PT substrate at fixed temperatures of (a) 300, (b) 270, (c) 240, (d) 210, (e) 180, and (f) 120 K.

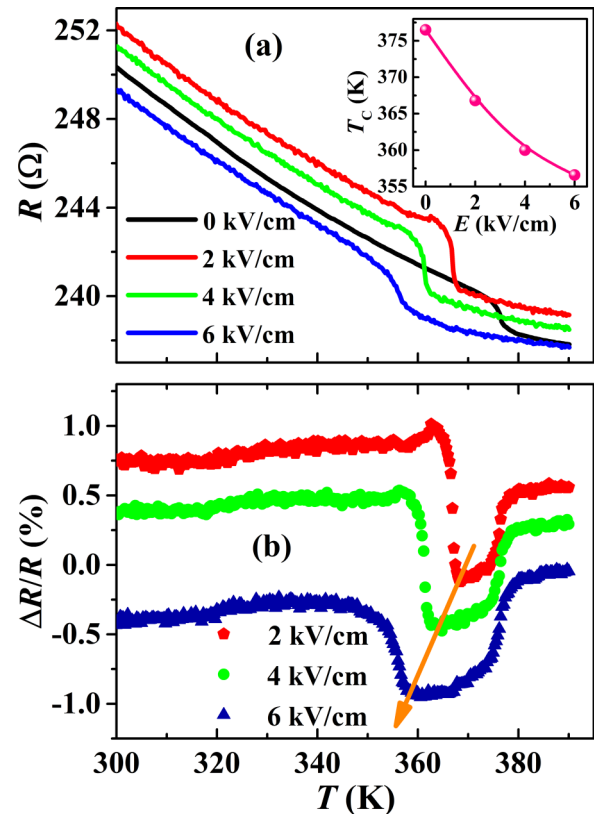FIG. 6. (a) Temperature dependence of the resistance of the 60-nm SIO film under the application of zero electric field and electric fields to the PMN-PT in the high-temperature region. Inset: the temperature where the resistance of the 60-nm SIO film changes abruptly as a function of the electric fields. (b) Temperature dependence of $\Delta R/R$ of the 60-nm SIO film under the application of electric fields to the PMN-PT substrate.
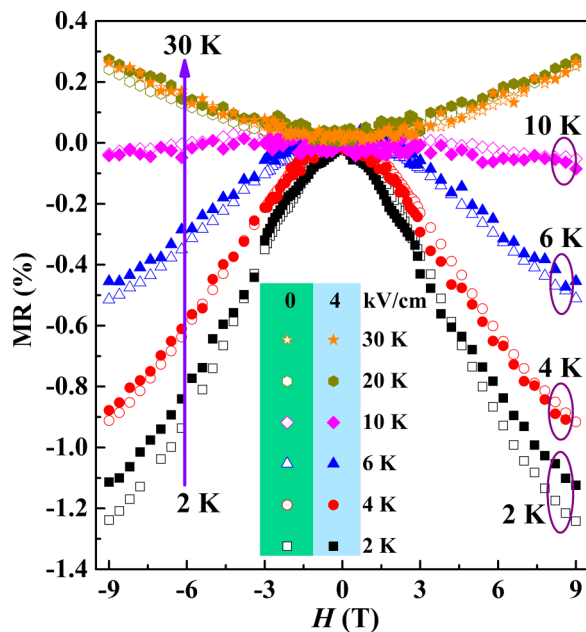
FIG. 7. MR of the 60-nm SIO film as a function of the magnetic field H, as measured at various fixed temperatures when a zero electric field and an electric field of 4 kV/cm were applied to the PMN-PT substrate.

defined as $\text{MR} = [R(H) - R(0)]/R(0) \times 100\%$, where $R(H)$ and $R(0)$ are the resistances of the SIO film under magnetic fields and zero magnetic fields, respectively. The negative MR at lower temperatures is similar to the previous reports and is caused by the magnetic field suppressing the localization interference of back-scattered waves.[13] With increasing temperature from 2 to 30 K, MR decreases and almost vanishes at $T = 10$ K. However, when the temperature is raised to $T = 20$ K, the sign of MR changes to positive, which is similar to the one found in normal metallic systems and may be attributed to the Lorentz contribution.[13,42] With an applied electric field of 4 kV/cm to the PMN-PT substrate at 2 K, MR becomes slightly smaller than that under zero electric field, for example, MR at $H = 9$ T is reduced by 14.2% upon the application of $E = 4$ kV/cm to the PMN-PT substrate, which suggests that the electric-field-induced in-plane compressive strain reduces the influence of quantum corrections to conductivity.

IV. CONCLUSIONS

In summary, $SrIrO_3$ thin films with various thicknesses were epitaxially grown on piezoelectric PMN-PT single-crystal substrates using the pulse laser deposition method. The lattice strain, resistance, and magnetoresistance of $SrIrO_3$ films could be *in situ* tuned and modulated by the ferroelectric domain rotation-induced strain near the coercive field, piezoelectric strain, and rhombohedral-to-tetragonal structural phase transition of the PMN-PT substrate. With decreasing temperature, the shape of the resistance vs electric field curves evolves from a symmetrical butterflylike to tilted and, finally, to an almost linear shape because of the increase in the

coercive field of the PMN-PT with decreasing temperature. At $T = 2$ K, upon application of $E = 4$ kV/cm to the PMN-PT layer, the negative MR of the $SrIrO_3$ film is reduced by approximately 14.2%, indicating an in-plane compressive strain-induced suppression of the influence of quantum corrections to conductivity. Our work demonstrates that the combination of 5d iridates with piezoelectric PMN-PT could provide an alternative approach to probe into the lattice strain effects of 5d iridates.

SUPPLEMENTARY MATERIAL

See the supplementary material for more detailed characterization and transport results.

AUTHOR DECLARATIONS

Conflict of Interest

The authors have no conflicts to disclose.

Author Contributions

Shuang-Shuang Li: Data curation (lead); Writing – original draft (lead). **Ying Zhang:** Writing – original draft (equal). **Jing-Shi Ying:** Writing – original draft (equal). **Zao-Cai Wang:** Writing – original draft (equal). **Jian-Min Yan:** Writing – original draft (equal). **Guan-Yin Gao:** Writing – original draft (equal). **Mao Ye:** Validation (equal). **Ren-Kui Zheng:** Writing – original draft (equal).

DATA AVAILABILITY

The data that support the findings of this study are available from the corresponding authors upon reasonable request.

REFERENCES

[1]Z. M. Tian, Y. Kohama, T. Tomita, H. Ishizuka, T. K. Hsieh, J. J. Ishikawa, K. Kindo, L. Balents, and S. Nakatsuji, "Field-induced quantum metal-insulator transition in the pyrochlore iridate $Nd_2Ir_2O_7$," Nat. Phys. **12**, 134–138 (2016).

[2]X. G. Wan, A. M. Turner, A. Vishwanath, and S. Y. Savrasov, "Topological semimetal and Fermi-arc surface states in the electronic structure of pyrochlore iridates," Phys. Rev. B **83**, 205101 (2011).

[3]C. Wang, H. Seinige, G. Cao, J. S. Zhou, J. B. Goodenough, and M. Tsoi, "Anisotropic magnetoresistance in antiferromagnetic Sr_2IrO_4," Phys. Rev. X **4**, 041034 (2014).

[4]M. Jenderka, J. Barzola-Quiquia, Z. P. Zhang, H. Frenzel, M. Grundmann, and M. Lorenz, "Mott variable-range hopping and weak antilocalization effect in heteroepitaxial Na_2IrO_3 thin films," Phys. Rev. B **88**, 045111 (2013).

[5]X. C. Huang, L. X. Zhao, Y. J. Long, P. P. Wang, D. Chen, Z. H. Yang, H. Liang, M. Q. Xue, H. M. Weng, Z. Fang, X. Dai, and G. F. Chen, "Observation of the chiral-anomaly-induced negative magnetoresistance in 3D weyl semimetal TaAs," Phys. Rev. X **5**, 031023 (2015).

[6]A. Shitade, H. Katsura, J. Kuneš, X. L. Qi, S. C. Zhang, and N. Nagaosa, "Quantum spin Hall effect in a transition metal oxide Na_2IrO_3," Phys. Rev. Lett. **102**, 256403 (2009).

[7]S. Thirupathaiah, R. Jha, B. Pal, J. S. Matias, P. K. Das, I. Vobornik, R. A. Ribeiro, and D. D. Sarma, "Temperature independent band structure of WTe_2 as observed from ARPES," Phys. Rev. B **96**, 165149 (2017).

06 January 2025 06:51:21

[8]Y. K. Kim, N. H. Sung, J. D. Denlinger, and B. J. Kim, "Observation of a d-wave gap in electron-doped Sr$_2$IrO$_4$," Nat. Phys. **12**, 37–41 (2016).

[9]B. J. Kim, H. Jin, S. J. Moon, J. Y. Kim, B. G. Park, C. S. Leem, J. Yu, T. W. Noh, C. Kim, S. J. Oh, J. H. Park, V. Durairaj, G. Cao, and E. Rotenberg, "Novel J$_{eff}$=1/2 mott state induced by relativistic spin-orbit coupling in Sr$_2$IrO$_4$," Phys. Rev. Lett. **101**, 076402 (2008).

[10]L. Y. Zhang, Q. F. Liang, Y. Xiong, B. B. Zhang, L. Gao, H. D. Li, Y. B. Chen, J. Zhou, S. T. Zhang, Z. B. Gu, S. H. Yao, Z. M. Wang, Y. Lin, and Y. F. Chen, "Tunable semimetallic state in compressive-strained SrIrO$_3$ films revealed by transport behavior," Phys. Rev. B **91**, 035110 (2015).

[11]B. J. Kim, H. Ohsumi, T. Komesu, S. Sakai, T. Morita, H. Takagi, and T. Arima, "Phase-sensitive observation of a spin-orbital mott state in Sr$_2$IrO$_4$," Science **323**, 1329 (2009).

[12]G. Cao, Y. Xin, C. S. Alexander, J. E. Crow, P. Schlottmann, M. K. Crawford, R. L. Harlow, and W. Marshall, "Anomalous magnetic and transport behavior in the magnetic insulator Sr$_3$Ir$_2$O$_7$," Phys. Rev. B **66**, 214412 (2002).

[13]A. Biswas, K. S. Kim, and Y. H. Jeong, "Metal insulator transitions in perovskite SrIrO$_3$ thin films," J. Appl. Phys. **116**, 213704 (2014).

[14]W. Guo, D. X. Ji, Z. B. Gu, J. Zhou, Y. F. Nie, and X. Q. Pan, "Engineering of octahedral rotations and electronic structure in ultrathin SrIrO$_3$ films," Phys. Rev. B **101**, 085101 (2020).

[15]K. Sen, D. Fuchs, R. Heid, K. Kleindienst, K. Wolff, J. Schmalian, and M. Le Tacon, "Strange semimetal dynamics in SrIrO$_3$," Nat. Commun. **11**, 4270 (2020).

[16]S. J. Moon, H. Jin, K. W. Kim, W. S. Choi, Y. S. Lee, J. Yu, G. Cao, A. Sumi, H. Funakubo, C. Bernhard, and T. W. Noh, "Dimensionality-controlled insulator-metal transition and correlated metallic state in 5d transition metal oxides Sr$_{n+1}$Ir$_n$O$_{3n+1}$ (n = 1, 2, and ∞)," Phys. Rev. Lett. **101**, 226402 (2008).

[17]M.-W. Yoo, J. Tornos, A. Sander, L.-F. Lin, N. Mohanta, A. Peralta, D. Sanchez-Manzano, F. Gallego, D. Haskel, J. W. Freeland, D. J. Keavney, Y. Choi, J. Strempfer, X. Wang, M. Cabero, H. Babu Vasili, M. Valvidares, G. Sanchez-Santolino, J. M. Gonzalez-Calbet, A. Rivera, C. Leon, S. Rosenkranz, M. Bibes, A. Barthelemy, A. Anane, E. Dagotto, S. Okamoto, S. G. E. te Velthuis, J. Santamaria, and J. E. Villegas, "Large intrinsic anomalous Hall effect in SrIrO$_3$ induced by magnetic proximity effect," Nat. Commun. **12**, 3283 (2021).

[18]A. K. Jaiswal, D. Wang, V. Wollersen, R. Schneider, M. L. Tacon, and D. Fuchs, "Direct observation of strong anomalous Hall effect and proximity-induced ferromagnetic state in SrIrO$_3$," Adv. Mater. **34**, 2109163 (2022).

[19]L. Hao, D. Meyers, C. Frederick, G. Fabbris, J. Y. Yang, N. Traynor, L. Horak, D. Kriegner, Y. Choi, J.-W. Kim, D. Haskel, P. J. Ryan, M. P. M. Dean, and J. Liu, "Two-dimensional J$_{eff}$ = 1/2 antiferromagnetic insulator unraveled from interlayer exchange coupling in artificial perovskite iridate superlattices," Phys. Rev. Lett. **119**, 027204 (2017).

[20]A. G. Zaitsev, A. Beck, A. K. Jaiswal, R. Singh, R. Schneider, M. Le Tacon, and D. Fuchs, "Anomalous pressure dependence of the electronic transport and anisotropy in SrIrO$_3$ films," J. Phys.: Condens. Matter **32**, 345601 (2020).

[21]Y. F. Nie, P. D. King, C. H. Kim, M. Uchida, H. I. Wei, B. D. Faeth, J. P. Ruf, J. P. Ruff, L. Xie, X. Pan, C. J. Fennie, D. G. Schlom, and K. M. Shen, "Interplay of spin-orbit interactions, dimensionality, and octahedral rotations in semimetallic SrIrO$_3$," Phys. Rev. Lett. **114**, 016401 (2015).

[22]V. Singh and J. J. Pulikkotil, "Cooperative effects of lattice and spin-orbit coupling on the electronic structure of orthorhombic SrIrO$_3$," J. Phys.: Condens. Matter **27**, 335502 (2015).

[23]A. Biswas and Y. H. Jeong, "Effects of substrate temperature on the unusual non-Fermi liquid metal to insulator transition in perovskite SrIrO$_3$ thin films," J. Phys. D: Appl. Phys. **48**, 135303 (2015).

[24]Y. V. Kislinskii, G. A. Ovsyannikov, A. M. Petrzhik, K. Y. Constantinian, N. V. Andreev, and T. A. Sviridova, "Structure and electron transport of strontium iridate epitaxial films," Phys. Solid State **57**, 2519–2523 (2015).

[25]J. H. Gruenewald, J. Nichols, J. Terzic, G. Cao, J. W. Brill, and S. S. A. Seo, "Compressive strain-induced metal-insulator transition in orthorhombic SrIrO$_3$ thin films," J. Mater. Res. **29**, 2491–2496 (2014).

[26]D. J. Groenendijk, N. Manca, G. Mattoni, L. Kootstra, S. Gariglio, Y. Huang, E. van Heumen, and A. D. Caviglia, "Epitaxial growth and thermodynamic stability of SrIrO$_3$/SrTiO$_3$ heterostructures," Appl. Phys. Lett. **109**, 041906 (2016).

[27]G. Wan, J. W. Freeland, J. Kloppenburg, G. Petretto, J. N. Nelson, D.-Y. Kuo, C.-J. Sun, J. Wen, J. T. Diulus, G. S. Herman, Y. Dong, R. Kou, J. Sun, S. Chen, K. M. Shen, D. G. Schlom, G.-M. Rignanese, G. Hautier, D. D. Fong, Z. Feng, H. Zhou, and J. Suntivich, "Amorphization mechanism of SrIrO$_3$ electrocatalyst: How oxygen redox initiates ionic diffusion and structural reorganization," Sci. Adv. **7**, eabc7323 (2021).

[28]C. M. Guo, H. Zhang, and X. L. Cheng, "Different magnetic responses induced by unequal oxygen vacancies in SrIrO$_3$," Physica B **596**, 412391 (2020).

[29]M. Xu, T. W. Chen, J. M. Yan, L. Guo, H. Wang, G. Y. Gao, H. S. Luo, Y. Chai, and R. K. Zheng, "Tunable magnetoresistance and charge carrier density in Cr:In$_2$O$_3$/PbMg$_{1/3}$Nb$_{2/3}$O$_3$-PbTiO$_3$ ferroelectric field-effect devices," Phys. Rev. Appl. **13**, 064006 (2020).

[30]C. R. Qiu, B. Wang, N. Zhang, S. J. Zhang, J. F. Liu, D. Walker, Y. Wang, H. Tian, T. R. Shrout, Z. Xu, L. Q. Chen, and F. Li, "Transparent ferroelectric crystals with ultrahigh piezoelectricity," Nature **577**, 350–354 (2020).

[31]L. Y. Zhang, H. Y. Wu, J. Zhou, F. X. Wu, Y. B. Chen, S. H. Yao, S. T. Zhang, and Y. F. Chen, "TEM study of SrIrO$_3$ thin films with various thicknesses grown on (001) SrTiO$_3$ substrates synthesized by pulsed laser deposition," Appl. Surf. Sci. **280**, 282–286 (2013).

[32]L. Y. Zhang, Q. F. Liang, Y. Xiong, B. B. Zhang, L. Gao, H. D. Li, Y. B. Chen, J. Zhou, S. T. Zhang, Z. B. Gu, S. H. Yao, Z. M. Wang, Y. Lin, and Y. F. Chen, "Tunable semimetallic state in compressive-strained SrIrO$_3$ films revealed by transport behavior," Phys. Rev. B **92**, 039904 (2015).

[33]K. R. Kleindienst, K. Wolff, J. Schubert, R. Schneider, and D. Fuchs, "Structural properties and anisotropic electronic transport in SrIrO$_3$ films," Phys. Rev. B **98**, 115113 (2018).

[34]M. Zheng and R. K. Zheng, "Electric-field-tunable ferroelastic control of non-volatile resistivity and ferromagnetic switching in multiferroic La$_{0.67}$Ca$_{0.33}$MnO$_3$/[PbMg$_{1/3}$Nb$_{2/3}$O$_3$]$_{0.7}$[PbTiO$_3$]$_{0.3}$ heterostructures," Phys. Rev. Appl. **5**, 044002 (2016).

[35]R. K. Zheng, H. U. Habermeier, H. L. W. Chan, C. L. Choy, and H. S. Luo, "Effects of substrate-induced strain on transport properties of LaMnO$_{3+\delta}$ and CaMnO$_3$ thin films using ferroelectric poling and converse piezoelectric effect," Phys. Rev. B **81**, 104427 (2010).

[36]Q. X. Zhu, W. Wang, S. W. Yang, X. M. Li, Y. Wang, H. U. Habermeier, H. S. Luo, H. L. W. Chan, X. G. Li, and R. K. Zheng, "Coaction and competition between the ferroelectric field effect and the strain effect in Pr$_{0.5}$Ca$_{0.5}$MnO$_3$ film 0.67Pb(Mg$_{1/3}$Nb$_{2/3}$)O$_3$–0.33PbTiO$_3$ crystal heterostructures," Appl. Phys. Lett. **101**, 172906 (2012).

[37]D. Hirai, J. Matsuno, D. Nishio-Hamane, and H. Takagi, "Semimetallic transport properties of epitaxially stabilized perovskite CaIrO$_3$ films," Appl. Phys. Lett. **107**, 012104 (2015).

[38]Y,N Li, J. M. Yan, G. Y. Gao, L. Shi, F. F. Wang, Y. K. Liu, and R. K. Zheng, "Strain-mediated electric-field manipulation of superconducting properties of FeSe$_{0.5}$Te$_{0.5}$ thin films grown on piezoelectric single crystals," Thin Solid Films **660**, 171–174 (2018).

[39]M. Zheng, M. M. Yang, Q. X. Zhu, X. Y. Li, G. Y. Gao, R. K. Zheng, Y. Wang, X. M. Li, X. Shi, H. S. Luo, and X. G. Li, "Tunable interface strain coupling and its impact on the electronic transport and magnetic properties of La$_{0.5}$Ca$_{0.5}$MnO$_3$/Pb(In$_{1/2}$Nb$_{1/2}$)O$_3$–Pb(Mg$_{1/3}$Nb$_{2/3}$)O$_3$–PbTiO$_3$ multiferroic heterostructures," Phys. Rev. B **90**, 224420 (2014).

[40]J. P. Han and W. W. Cao, "Electric field effects on the phase transitions in [001]-oriented (1-x)Pb(Mg$_{1/3}$Nb$_{2/3}$)O$_3$-xPbTiO$_3$ single crystals with compositions near the morphotropic phase boundary," Phys. Rev. B **68**, 134102 (2003).

[41]Y. J. Yang, Z. L. Luo, M. Meng Yang, H. L. Huang, H. B. Wang, J. Bao, G. Q. Pan, C. Gao, Q. Hao, S. T. Wang, M. Jokubaitis, W. Z. Zhang, G. Xiao, Y. P. Yao, Y. K. Liu, and X. G. Li, "Piezo-strain induced non-volatile resistance states in (011)-La$_{2/3}$Sr$_{1/3}$MnO$_3$/0.7Pb(Mg$_{2/3}$Nb$_{1/3}$)O$_3$–0.3PbTiO$_3$ epitaxial heterostructures," Appl. Phys. Lett. **102**, 033501 (2013).

[42]J. S. Blakemore, *Solid State Physics* (Cambridge University Press, 1985).

06 January 2025 06:51:21